Lipophilic modification of Salirasib modulate the antiproliferative and antimigratory activity.

María Sol Ballari,[a,†] Exequiel O. J. Porta,[a,#,†] Evelyn Arel Zalazar,[b] Carla M. Borini Etichetti,[c] José M. Padrón,[d] Javier E. Girardini,*,[b] and Guillermo R. Labadie*,[a,e]

a. Instituto de Química Rosario (IQUIR), Universidad Nacional de Rosario-CONICET, Suipacha 531, S2002LRK, Rosario, Argentina.

b. Instituto de Inmunología Clínica y Experimental de Rosario (IDICER), Consejo Nacional de Investigaciones Científicas y Técnicas (CONICET). Suipacha 590, S2000LRJ, Rosario, Argentina.

c. Instituto Fisiología Experimental de Rosario (IFISE-CONICET), Facultad de Ciencias Bioquímicas y Farmacéuticas, Universidad Nacional de Rosario, Suipacha 531, 2000 Rosario, Argentina.

d. BioLab, Instituto Universitario de Bio-Orgánica "Antonio González" (IUBO-AG), Universidad de La Laguna, Apartado 456, E-38071, La Laguna, Spain

e. Departamento de Química Orgánica, Facultad de Ciencias Bioquímicas y Farmacéuticas, Universidad Nacional de Rosario, Rosario, Argentina.

[#] Current address: Department of Chemistry, Durham University, DH1 3LE, Durham, United Kingdom.

[†] The authors have contributed equally.

* Corresponding authors e-mails: labadie@iquir-conicet.gov.ar; girardini@idicer-conicet.gob.ar

Abstract:

Salirasib, or farnesylthiosalicylic acid (FTS), is a salicylic acid derivative with demonstrated antineoplastic activity. While designed as a competitor of the substrate S-farnesyl cysteine on Ras, it is a potent competitive inhibitor of isoprenylcysteine carboxymethyl transferase. Although different salirasib derivatives have been reported, the isoprenyl tail has not been modified. In this study, we used a series of synthetic salirasib analogues with lipophilic thioether modifications, including those with or without a 1,2,3-triazole linker, and tested their antiproliferative activity against six different solid tumor cell lines. We carried out a combination of bioassay, cheminformatics, and in silico ADME-Tox to identify new potent analogues. SAR analysis revealed structural and physicochemical features that enhance antiproliferative activity. Analogues with three or more isoprene units or a long aliphatic chain exhibited the most potent activity. Furthermore, we identified three compounds with superior antiproliferative activity than salirasib and similar potency compared to control anticancer drugs across all tested solid tumor cell lines. In addition, the behaviour of the collection on migration and invasion, the key processes in tumor metastasis, were also studied. Three analogs with specific antimigratory activity were identified with differential structural features.

The combination of the antiproliferative and antimigratory results prompts to propose that the modification on the thiol aliphatic/prenyl substituents can modulate the activity. Our findings provide valuable insight on the lipophilic salirasib analogues with enhanced antiproliferative activity against solid tumor cell lines. Also, we have been able to identify analogues with specific antimigratory activity that could be the starting points on the development of new antimetastatic agents.

Graphical abstract
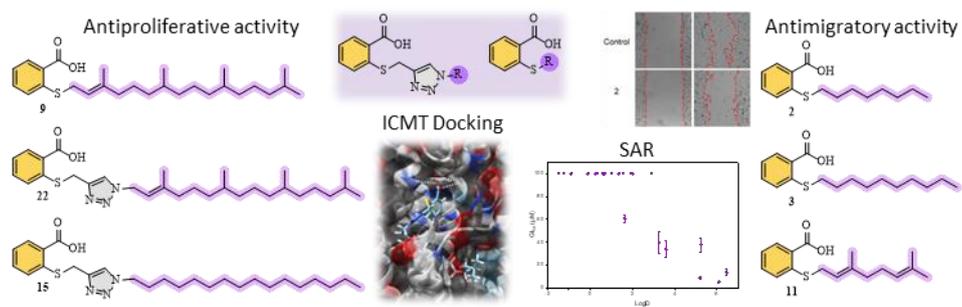
Keywords: Salirasib; 1,2,3-triazoles; Cancer; SAR studies; Cheminformatics; Docking; Cell Migration.

1. Introduction

Cancer is a large group of diseases characterized by the uncontrolled growth of abnormal cells in various organs and tissues, making it the second leading cause of death globally.[1] The prenylation pathway, which modifies proteins by attaching lipid groups, has been increasingly implicated in human cancer. Guanine binding proteins (G proteins) like Ras, Rap, Rho, and Rab, constitute the largest group of prenylated proteins.[2]

Protein prenylation occurs through a three-step post-translational process that facilitates protein-membrane association, a crucial step to trigger their oncogenic activities.[3] During the first step of prenylation, which takes place in the cytoplasm, an isoprenyl transferase such as Farnesyl Transferase (FTase) or Geranylgeranyl Transferase (GGTase), recognizes the CAAX motif at the protein's carboxyl terminus, where C represents cysteine, AA denotes two aliphatic amino acids, and X is a variable amino acid. Then, either a farnesyl (by the FTase) or a geranylgeranyl (by the GGTase) group is transferred to the cysteine of CAAX, forming a thioether bond with the corresponding sulfhydryl group. Following prenylation, the protein migrates to the endoplasmic reticulum, where a Ras Converting CAAX Endopeptidase 1 (RCE-1) cleaves the -AAX tail, leaving the C-terminus with an isoprenylcysteine. This motif is recognized by an Isoprenylcysteine Carboxymethyl Transferase (ICMT), which catalyzes the transfer of a methyl group from *S*-adenosyl-L-methionine to the isoprenylated carboxyl terminus, forming an ester. This modification on substrate proteins promotes membrane anchoring and regulates its interaction with other protein partners.[4]

Among ICMT targets, Ras proteins have attracted particular attention due to their crucial role in carcinogenesis.[5] These proteins are engaged in signal transduction pathways that regulate cell growth and differentiation. Mutations in Ras proteins can turn them into oncogenic forms and are found in approximately 19% of all human tumors, including more than 80% of pancreatic cancers and 45% of colon cancers.[6] In addition, several Rho GTPases, including RhoA and Rac1, are also ICMT targets. *In vitro* studies have shown that reduced migration and invasion of breast cancer cells upon ICMT pharmacological inhibition was associated with impairment of RhoA and Rac1 activity.[7]

Several lines of evidence implicate ICMT in mechanisms of oncogenesis. Our previous work has shown that ICMT expression is repressed by the p53 tumor suppressor. Accordingly, cancer patients classified as wild-type p53 showed reduced ICMT levels compared to those bearing p53 mutations.[2] Conversely, ICMT expression is induced by tumor-associated p53 point mutants. P53 mutations are among the most frequent

alterations found in human cancer, and p53 point mutants actively cooperate with the acquisition of aggressive tumor traits.[8] Furthermore, ICMT overexpression has been shown to enhance tumor development in a xenograft model of H1299 non-small cell lung carcinoma cells.[9] Noteworthy, pharmacological ICMT inhibition has been shown to reduce tumor growth in xenograft models of different cancer cell lines.[9] This data supports the notion that ICMT is intimately related to oncogenic mechanisms and underscore its relevance as a therapeutic target.

A strategy that has gained relevance over the years is the development of inhibitors for the post-translational prenylation process at any of its three stages. Ftase inhibitors have been successful in pre-clinical studies,[10] but many of them failed in phase III. This is attributed to the fact that many Ras mutants (e.g, KRAS, NRAS, etc.) have proven to be good GGTase substrates when Ftase is inhibited.[3] However, FTase inhibitors for Ras mutants that did not show this effect in clinical trials are promising anticancer drug candidates.[11] The inhibition of RCE-1 was also studied,[12] but experiments in mice have shown discouraging results,[13] setting this target aside. By contrast, ICMT inhibitors have gained relevance among the Ras-dependent anti-cancer agents.[4] Within the ICMT inhibitors, the most relevant candidates are the indole cysmethynil[14] and the substrate analogue salirasib (**Fig. 1**).[15,16]

Salirasib, also known as farnesylthiosalicylic acid (FTS), is a salicylic acid derivative that has demonstrated potent antitumor and antineoplastic activity. Originally designed as a competitor of the substrate *S*-farnesyl cysteine on Ras,[17] salirasib also acts as a potent competitive inhibitor of ICMT. Therefore, salirasib selectively disrupts the association of activated Ras proteins with the plasma membrane.[18] These precedents set the basis for studying this compound as a promising candidate for the treatment of a wide range of cancers, such as pancreas, lung, colon, among others. Preclinical and phase I clinical trials in mutant Ras-positive cancer patients showed that salirasib could be well tolerated, with no significant side effects and with good pharmacological parameters.[19] There is still little information about phase II clinical trials, which would require dosage increments to improve results.[20] Hence, the scientific community is still working on salirasib structural optimization to generate new leads, which could help to move forward to later stages of trials.[21,22]
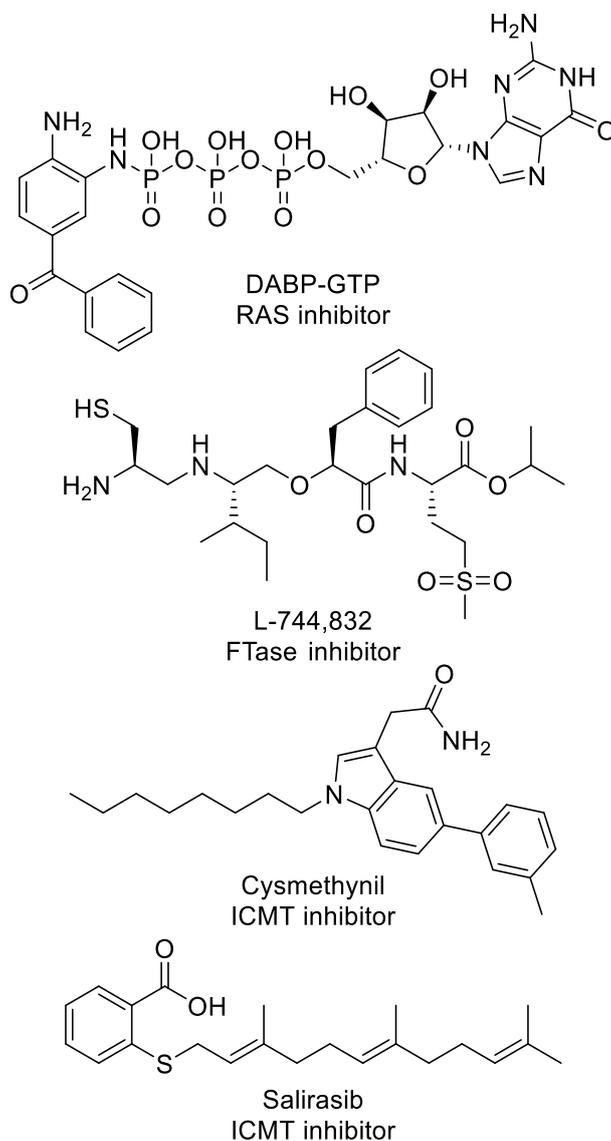
Fig. 1. RAS-related anti-cancer agents.

Salirasib has limited bioavailability and chemical stability, which has prompted the search for novel analogues with improved properties. We have previously reported the synthesis and antimalarial activity of salirasib analogues as a means of drug repurposing.[23] This compound collection consists of thiosalicylic acid (TSA) derivatives. The library has two variables based on the absence (compounds **1 – 13, Fig. 2**) or presence (compounds **14 – 25, Fig. 2**) of a 1,2,3-triazole linker inserted between the TSA and the non-polar R substituent. In this opportunity, the antiproliferative activity of this library in human solid tumor cell lines was evaluated. Additionally, we searched for compounds able to inhibit cell migration and we investigated the potential modes of action of these compounds. Our findings provide valuable insights into the structure-activity relationships of salirasib analogues and may contribute to the development of new and effective anticancer agents.
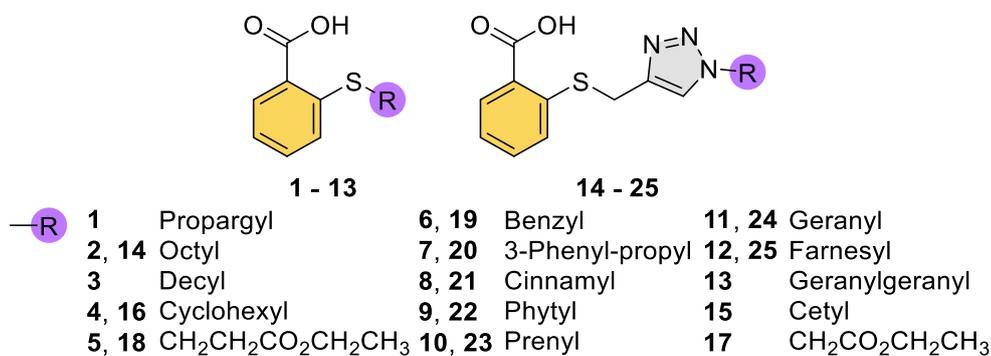
Fig. 2. Salirasib analogues under study in this work.

2. Results and discussion

2.1. Salirasib analogues and their physicochemical profile as potential ICMT inhibitors

As we previously reported,[23] the salirasib analogues **1** - **13** were easily prepared using thiosalicylic acid, the appropriate halide as an electrophile, and guanidinium carbonate as the base, in refluxing. Compounds **14** – **25** were synthesized using click chemistry (CuACC) between propargyl thiosalicylic acid **1** and the appropriate azide. Structural diversity was achieved by introducing different R lipophilic substituents, resulting in a diverse library with appropriate physicochemical properties distribution. However, the use of allylic azides (**23**, **24**, and **25**) resulted in an inseparable mixture of regioisomers due to a spontaneous [3,3]-sigmatropic Winstein rearrangement.[24,25]

Since our compounds were structurally related to the ICMT inhibitor salirasib, we compared the physicochemical properties of our compound collection with reported ICMT inhibitors. We identified a total of 467 reported *Hs*ICMT inhibitors from the ChemBL database.[26] Afterwards, the Osiris DataWarrior platform[27] was used to calculate the physicochemical properties of the *Hs*ICMT inhibitors and our synthetic library. Normalized histograms of molecular weight (MW), total surface area, cLogP and cLogS are shown in **Fig. 3**. The figure compares the distribution of the different properties among compounds belonging to the previously reported inhibitors database and our set of salirasib analogues. It can be observed that the property distributions are very similar between both sets. For the reported *Hs*ICMT inhibitors database, the maximum compound counts were at MW = 350 to 400 Da, total surface area = 250 to 300 Å^2, cLogP = 4.5 to 5, and cLogS = -5 to -4.5. On the other hand, for our set of compounds, maximum counts were at MW = 250 to 350 Da, total surface area = 200 to 250 Å^2, cLogP = 3 to 3.5, and cLogS = -4.5 to -4. The most frequent values for each property were slightly lower for the salirasib analogues library, but overall, our collection covers a

wide range of desirable physicochemical properties to offer a promising antiproliferative activity against solid tumor cell lines.
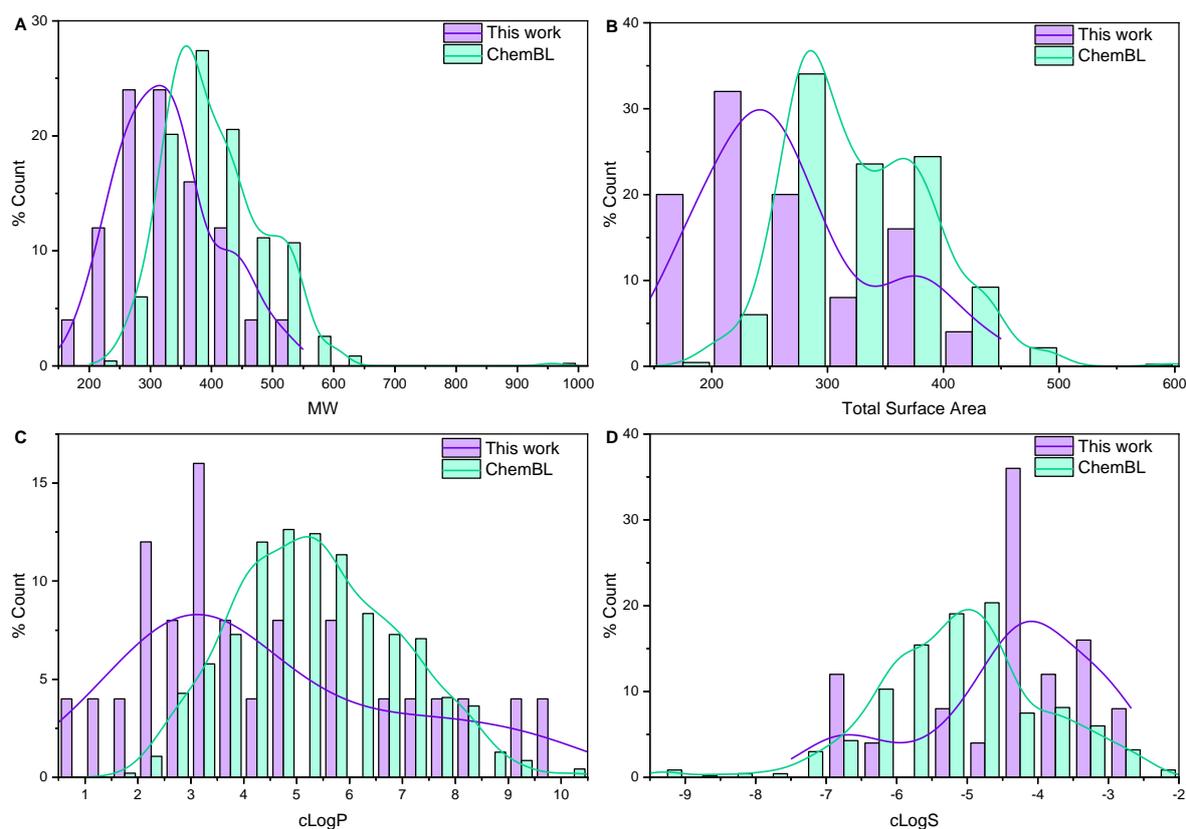
Fig. 3. Normalized physicochemical properties distribution for ChemBL dataset (ChemBL, green bars) and salirasib analogues dataset (this work, violet bars). Distributions were fitted to Kernel Smooth function (green and violet lines for the datasets of ChemBL and this work, respectively). A) MW; B) Total surface area; C) cLogP; D) cLogS.

2.2. *In vitro* antiproliferative activity

The *in vitro* antiproliferative activity of compounds **1** - **25** was evaluated against a panel of six human solid tumor cell lines including A549 (non-small cell lung), HeLa (cervix), SW1573 (non-small cell lung), T-47D (breast), HBL-100 (breast), and H1299 (non-small cell lung). The concentration of the compound that inhibits 50% of the culture growt (GI_{50}s) were determined and results are presented in **Table 1**.

Detailed analysis of **Table 1** revealed that seven (including salirasib), out of the twenty-five compounds assayed, were active (i.e., GI_{50} < 100 µM) against most of the cell lines, with similar trends among them. The GI_{50}s of the active analogues were around 102 µM for the less potent, falling to 4.3 µM for the most effective one, with no significant differences between the cell lines.

Table 1. Antiproliferative activity most active analogues ($GI_{50} < 100$ μM).
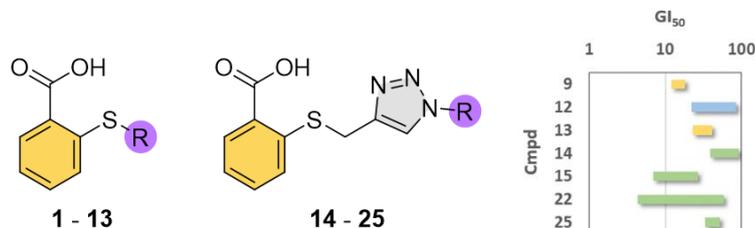
Compound	Family	R	GI_{50} (μM)					
			A549	HeLa	SW1573	T-47D	HBL-100	H1299
9	*S*-R	Phytyl	14 ± 2.4	12 ± 2.4	15 ± 3.3	18 ± 1.3	14 ± 1.9	> 100
12	*S*-R	Farnesyl (Salirasib)	34 ± 7.0	34 ± 5.1	41 ± 10	42 ± 9.3	22 ± 5.4	85 ± 10
13	*S*-R	Geranylgeranyl	38 ± 6.1	29 ± 2.9	37 ± 6.7	41 ± 0.6	23 ± 1.8	-
14	*S*-triazolyl-R	Octyl	61 ± 3.4	39 ± 6.5	47 ± 7.9	93 ± 11	40 ± 0.3	> 100
15	*S*-triazolyl-R	Cetyl	9.2 ± 0.7	6.9 ± 0.04	9.3 ± 0.03	20 ± 5.9	14 ± 1.2	27 ± 5
22	*S*-triazolyl-R	Phytyl	5.4 ± 0.7	4.3 ± 1.3	5.8 ± 0.6	9.6 ± 1.3	10 ± 1.1	59 ± 14
25	*S*-triazolyl-R	Farnesyl	40 ± 9.9	33 ± 3.3	40 ± 6.3	52 ± 11	33 ± 0.9	102 ± 12
Cisplatin			4.9 ± 0.2	2.0 ± 0.3	3.0 ± 0.4	15 ± 2.3	1,9 ± 0.2	
Etoposide			1.5 ± 0.3	3.3 ± 1.6	14 ± 1.5	22 ± 5.5	1.4 ± 0.1	
Camptothecin			-	0.6 ± 0.4	0.3 ± 0.1	2.0 ± 0.5	0.2 ± 0.1	

All the compounds were tested at a maximum concentration of 100 μM. Values are mean ± standard deviation of two to three independent experiments. (-): not tested

In particular, the phytyl analogue **22** is the most active compound in this collection, displaying the best antiproliferative activity against five of the cell lines tested. Indeed, compared with salirasib, it is 6.3 times more active in A549, 8 times more active in HeLa, 7 times more active in SW1573, 4.4 times more active in T-47D, 2.2 times more active in HBL-100, and 1.4 times more active in H1299. Notably, this compound exhibits biological activity against the various cell lines in a similar order to the control drugs cisplatin and etoposide. **Fig. 4** shows the trend map of antiproliferative activities of all active compounds, with salirasib as the reference point for comparison.

Fig 4. Trend map of active compounds against tumor cell lines (A549, HeLa, SW1573, T-47D, HBL-100, and H1299). The green triangles show an improvement in its biological activity compared with salirasib, while the red triangles show a loss of activity. The numbers reflect the improvement or loss in its activity (GI_{50}salirasib / GI_{50}product).

All the compounds that affect cell viability share a common feature, which is that the sulfur atom is bound to an electron-deficient carbon. We hypothesize that the presence of an allyl or a 4-triazolyl methylene

adjacent to the sulfur atom could be playing an important role in the antiproliferative activity observed. It was noteworthy that all the active analogues are substituted with long lipophilic chains.

Among the active compounds with 1,2,3-triazole ring, the octyl group was the shortest R substituent, while among active compounds without heterocycle, farnesyl was the shortest R substituent. Phytyl, and cetyl were the R chains that provided the best activities. Interestingly, the phytyl (**9**, **22**) and cetyl (**15**) analogues, both 16 carbons long, were more active than salirasib (**12**), as indicated by the GI_{50} range plot (**Table 1**).

The thiosalicylic acid S-substituted with a N1-phytyl-1,2,3-triazolyl group has shown the best performance among the tested compounds. Additionally, the phytyl S-substitution has previously been studied in cysteine analogues and produced promising results as non-steroidal anti-inflammatory agents targeting ICMT.[28,29] The phytyl-substituted analogs (with and without the triazole moiety) were the most active compounds in the series when tested as antimalarial agents. These compounds also showed similar potencies compared to the tested tumor cell lines. Compounds **9** and **22** have an IC_{50} in *P. falciparum* of 13.40 ± 1.53 µM, and 9.75 ± 1.97 µM, respectively.[23] Those results reinforce the hypothesis that the triazolyl-phytyl group provides additional interactions with the molecular target of the thiosalicylic acid thioethers. To the best of our knowledge, the triazolyl-isoprenyl S-substitution of cysteine analogues have not been reported as antiproliferative agents. Based on your findings, it would be an interesting scaffold to explore in the development of novel antiproliferative agents.

2.3. Migration and invasion inhibition experiments

ICMT inhibition can reduce migration and invasion, which are key phenotypes of metastatic tumor cells.[7] Metastatic spread relies on the ability of cells from the primary tumor to invade and move through the adjacent tissue to reach circulation and colonize distant sites. Metastasis is the cause of death in the vast majority of solid tumors. Therefore, drugs able to counteract cancer cell migration and invasion may contribute to prevent disease progression. We wondered if compounds that did not show antiproliferative activity could affect migration and invasion *in vitro*. To identify molecules able to affect cell migration, we performed wound healing assays on H1299 cells treated with compounds from our collection (Supplementary Figure **S6**). This cell line derives from a lymph node metastasis and has been extensively used as a model of metastatic cells both *in vitro* and *in vivo*. Our results showed that treatment with compounds **2** (S-octyl), **3** (S-decyl) and **11** (S-geranyl) significantly reduced cell migration (**Fig. 6**). Interestingly, compounds **14** (S-triazolyl-octyl) and

10

24 (S-triazolyl-geranyl), containing with the same R substituents as compounds **2** and **11**, but with a 1,2,3-triazole linker, did not show any effect on cell migration (Supplementary Figure **S6**). These results indicate that the 1,2,3-triazole linker abolished the migration inhibitory effect in the compounds, and that alkyl thioether derivatives are the crucial structural feature for the migration inhibitory activity.
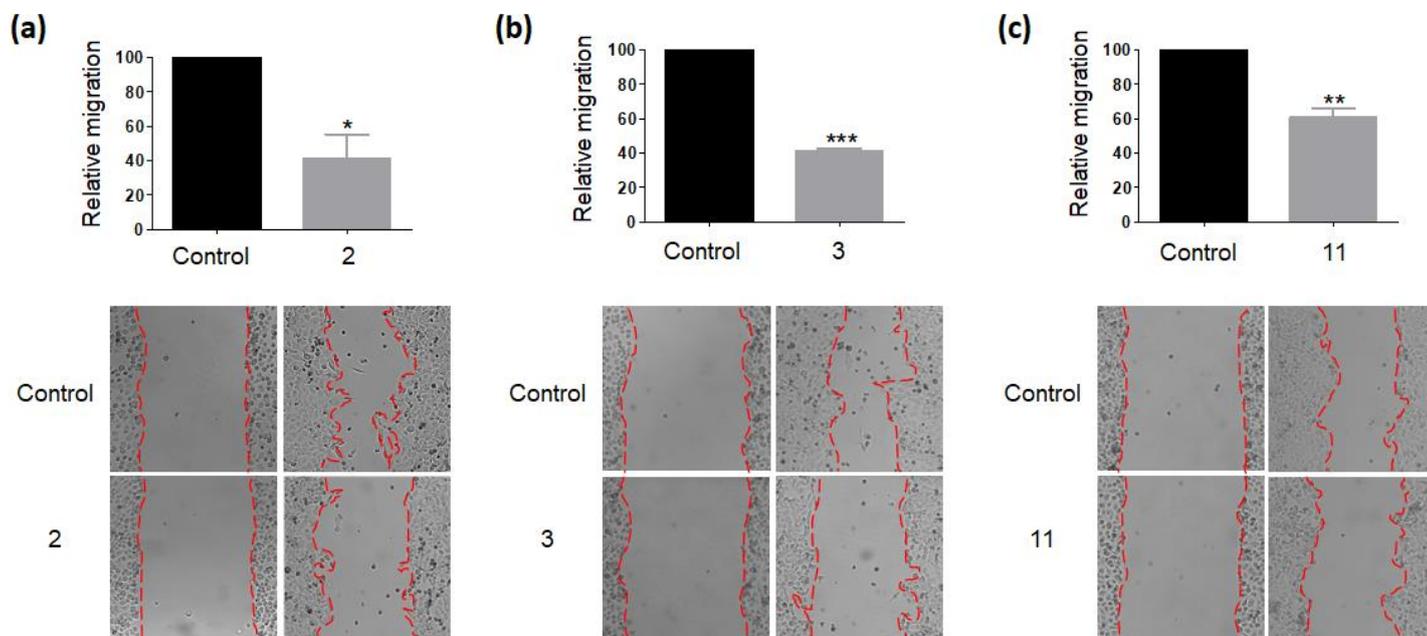
Fig. 6. Effect of S-alkyl thiosalicylic acid analogues on cancer cell migration. Wound healing assays on H1299 cells treated with the indicated compounds at 50 μM or DMSO dilution as control. Migrated distance is expressed relative to control condition. Lower panel: representative images of wound closure after 24 h. (a) Compound **2**, n = 3, p = 0.0269; (b) Compound **3**, n = 3, p = 0.0003; (c) Compound **11** n = 3, p = 0.0074.

Interestingly, salirasib has shown antiproliferative activity on T24 and BOY cells lines at high concentration (> 100 μM).[30] also shown antimigratory activity at 100 μM. Combinations of Exo2 and salirasib inhibited cell migration and invasion, with an inhibitory effect of co-treatment much greater compared with the single drug effects.[31] That contrast with our results on salirasib that display a GI$_{50}$ of 85 $\pm$ 10 μM on the H1299 cell line and did not affect the migratory behavior on the experiment performed on the same cell line.

To further characterize the effect of these compounds, we performed *in vitro* invasion assays. We treated H1299 cells with the compounds and seeded them onto Matrigel coated filters in transwell inserts. Cells able to pass through the filters were stained and counted (**Fig. 7**). We found that compounds **2** and **11** significantly reduced the ability of cells to invade. Compound **3** did not show a significant effect on invasion under these conditions. These results suggest a different mechanism underlying the effect of compound **3**.
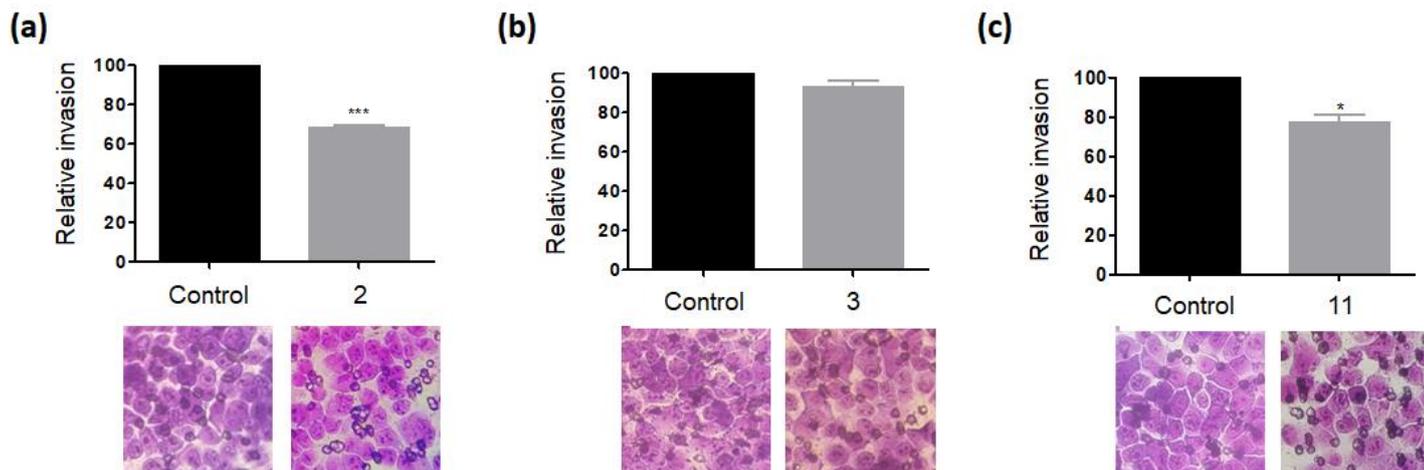
Fig. 7. Effect of S-alkyl thiosalicylic acid analogues on cancer cell invasion. Transwell assays on Matrigel-coated filters were performed with H1299 cells treated with the indicated compounds or DMSO dilution as control. Relative invasion is expressed as the percentage of migrated cells, treated with the indicated compounds, relative to migrated cells in the control condition. Lower panel: representative images of wound closure after 24 h. (a) Compound **2**, n = 3, p = 0.0009; (b) Compound **3**, n = 3, p = 0.0829; (c) Compound **11** n = 3, p = 0.0158.

2.3. Structure – Activity Relationship

To gain a deeper insight into the physicochemical profile of the collection and its biological response, properties against the GI50 for each cell line were plotted. These properties included molecular weight (MW), total surface area, LogD, and cLogS. This type of analysis can provide valuable information on the relationship between chemical properties and biological activity, helping to identify key factors that contribute to the observed activity.

Similar trends were observed for all cell lines, and SAR graphs for the A549 cell line were chosen to represent the panel (**Fig. 5**), while graphs for the remaining cell lines can be found in the Supporting Information.

Since our compounds collection contains ionizable groups that are charged at physiological pH, LogD (pH = 7)[32] is a better descriptor of lipophilicity than cLogP, leading us to use LogD for our SAR analysis. Remarkably, a clear "high activity" zone was observed for each property. More precisely, the compounds become active when MW > 350 Daltons, total surface area > 300 Å^2, LogD > 3, and cLogS < -5.

2.5. Docking studies.

As was previously stated, the most active compounds contain a 16-carbon R chain in their structures. Since farnesyl is a 12-carbon long, that could imply that the R chain would be occupying the isoprenyl

(hydrophobic) pocket in the ICMT. However, cetyl and phytyl, which are more flexible chains, could potentially fit in the lipophilic cavity and enhance activity. To corroborate this hypothesis, docking studies were conducted to examine the interaction between inhibitors and the molecular target. Since there is no crystallographic structure of *Hs*ICMT available, a predicted 3D-structure was generated by machine learning.
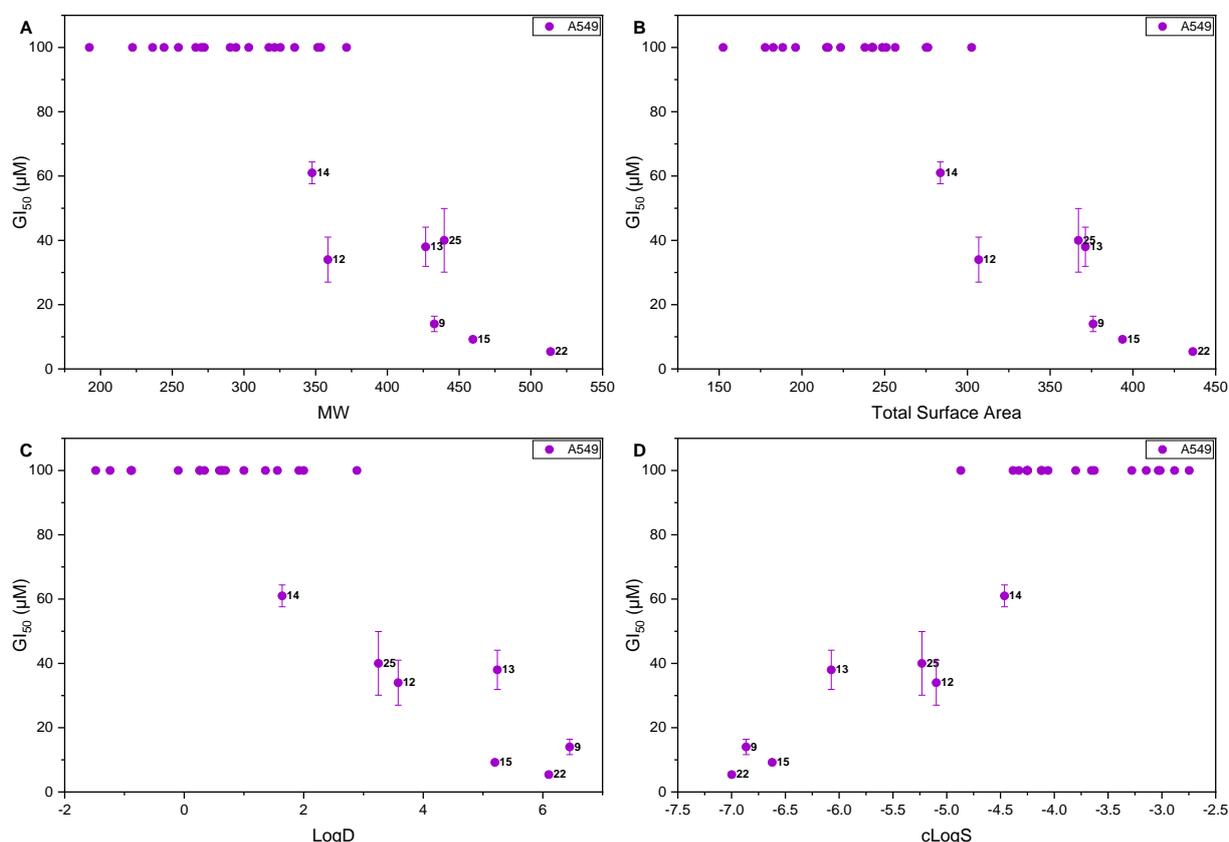
Fig. 5. Correlations between antiproliferative activity against A549 cell line and selected physicochemical properties. A) MW; B) Total Surface Area; C) LogD; D) cLogS.

AlphaFold[33] employs a machine learning approach that incorporates both physical and biological knowledge about protein structure. By leveraging multi-sequence alignments, AlphaFold is able to design a deep learning algorithm that can predict the structure of a protein with high accuracy. For these reasons, AlphaFold was used to generate a 3D structure of the *Hs*ICMT (UniProt ID: O60725). The predicted aligned error was less than 5 Å in the entire catalytic domain. Then, the predicted structure was compared with the crystallographic structure of ICMT from the beetle *Tribolium castaneum* (PDB codes: 5V7P and 5VG9). Human and beetle ICMT share the same predicted topology[34] and have 58% amino acid sequence identity within the region thought to contain the active site (amino acids 90–281). This enabled the identification of the active site and helped to guide further experimental studies to elucidate the mechanism of ICMT inhibition.

To investigate molecular interactions, docking simulations were performed using SwissDock. The simulations involved the predicted HsICMT, Salirasib (**12**), and all active analogues identified by GI_{50} and migration/invasion inhibitory effect (compounds **2**, **3**, **9**, **11**, **12**, **13**, **14**, **15**, **22**, and **25**), as well as a peptide substrate model (N-MeGly-Ala-Cys-S-Farnesyl). Additionally, two inactive compounds, **18** and **24**, were included as controls. These compounds lacked both biological activity (GI_{50}) and migratory/invasion effects.

The binding affinity values of the molecules were examined and compared with the binding affinity value of the substrate peptide (-10.25 Kcal/mol). Our results indicated that compounds with better antiproliferative activity profiles had higher binding affinity values (**Table S2**). Additionally, a more pronounced difference in energy values led to an increase in the antiproliferative activity. Conversely, molecules with values lower than that of the substrate peptide lost their antiproliferative activity at the concentrations tested. These findings suggest that the antiproliferative activity of the compounds may be associated, at least in part, with an inhibitory effect on ICMT. The three best compounds in the entire collection were found to have the highest binding affinity values: **9** (-11.32 Kcal/mol), **22** (-11.17 Kcal/mol), and **15** (-11.12 Kcal/mol).

In contrast, molecules that exert inhibitory effects on migration/invasion had lower affinity binding values than the substrate peptide, namely **2** (-8.96 Kcal/mol), **3** (-9.47 Kcal/mol), and **11** (-9.66 Kcal/mol). These results suggest that these molecules may be acting on other molecular targets, rather than ICMT.

The binding mode of the inhibitors showed that the carboxylate group coordinates with Arg246, which is located in M8. According to the reported X-ray structure,[35] Arg173 (in M6) and Arg246 are stabilised by hydrogen bonding networks, and two water molecules occupy the proposed location of the carboxylate. Furthermore, the interactions with the hydrophobic pocket of HsICMT were compared, revealing that different R side chains of the synthesised molecules with a higher proportion of sp^3 carbons (**9**, **15** and **22**) better fill the hydrophobic cavity (**Fig. 8**).

2.6. ADME-Tox.

Finally, both the antiploliferative (**9**, **12**, **13**, **14**, **15**, **22** and **25**) and antimigratory (**2**, **3** and **11**) compounds were assessed for their potential as leads and their ADME-Tox properties using web-based SwissADME,[36], Biotransformer[37] and pkCSM[38] (for more details, please see Supporting Information). The SwissADME analysis revealed that these compounds did not have any PAINS alerts, however, they did not fulfill the leadlikeness parameters for oral dosage. Only analogue **25** complied with the Lipinski, Ghose, Veber, Egan,

and Muegge parameters. Unfortunately, the most active compounds **9**, **15**, and **22** exhibited more druglikeness violations. Compound **22** did not fulfill the minimum requirements to be considered "druglike" and had the most alerts among the series, despite being the most active compound. The Biotransformer analysis showed that these compounds could be metabolized by the CYP450 complex, specifically, they could be substrates of CYP1A2, CYP2A6, CYP2B6, CYP2C8, CYP2C9, CYP2C19, CYP2D6, CYP2E1 and CYP3A4. The compounds could undergo aliphatic, allylic, or aromatic hydroxylations, thioether oxidation, arene epoxidation, or terminal desaturation. The production of more polar and soluble metabolites could facilitate a more effective elimination compared to their parent compounds.
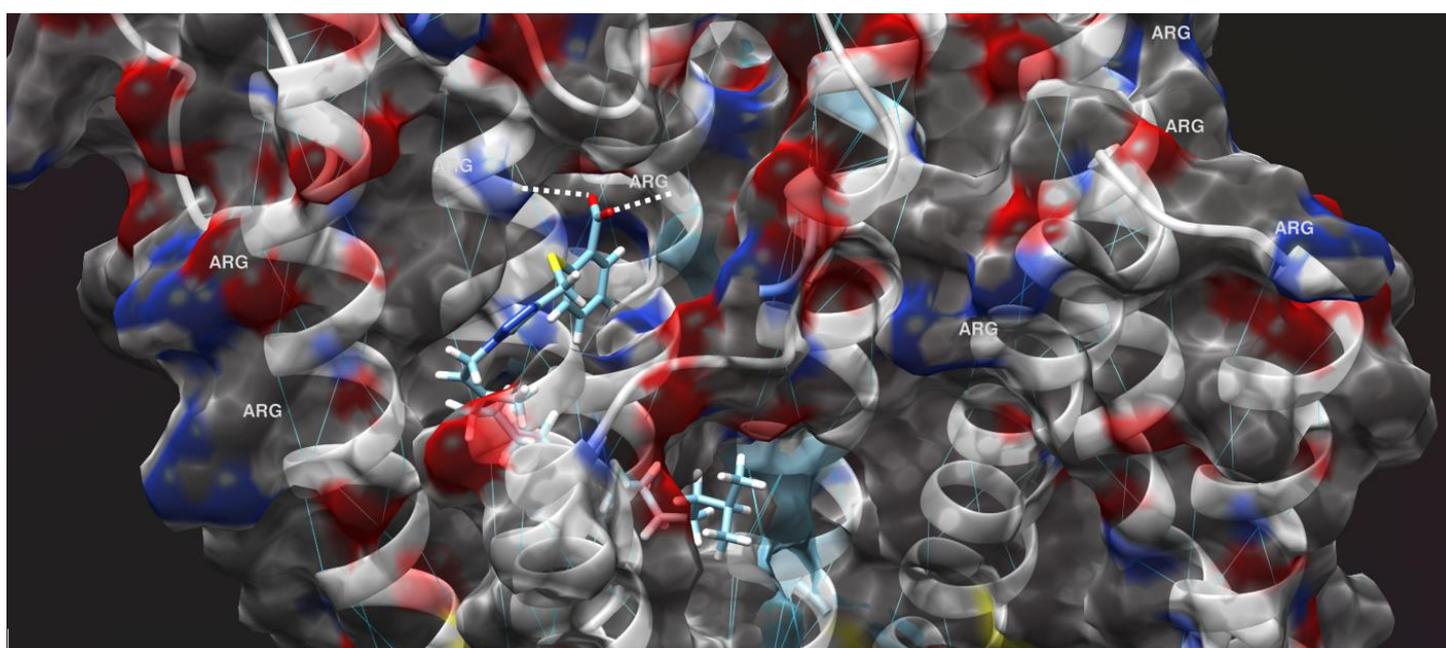
Fig. 8. Interaction between compound **22** and *Hs*ICMT. The charged carboxylate is stabilized by a hydrogen bond with Arg246 and Arg173 (white dotted lines). The lipid tail is embedded within the hydrophobic cavity.

The pkCSM prediction analysis revealed that all the compounds had favourable ADME-Tox properties. The absorption prediction indicated excellent intestinal absorption for all compounds, although compounds **14**, **15**, **22,** and **25** may experience reduced colorectal permeability The volumes of distribution (VDss) were relatively low, suggesting that the compounds may remain bound to serum proteins, which could hinder the distribution process. In terms of excretion parameters, the compounds showed better predictions than the reference compound salirasib (**12**), with the sole exception of compound **13**. None of the compounds were found to be mutagenic, however, compounds **11**, **14**, **15**, and **25** triggered hepatotoxicity alerts, and the antimigratory compounds **2**, **3** and **11** presented skin sensitisation alerts.

The study found that to achieve an improvement in the interaction with the possible target(s) and a substantial increase in the antiproliferative activity, the compounds needed to be more lipophilic, resulting in the most effective compounds being heavier, larger, more non-polar, and less water-soluble. This could potentially result in low oral bioavailability, limiting the dosage mode. However, to achieve a good *in vivo* biological effect, these types of compounds are more likely to require a formulation process, such as liposomes. This is not a disadvantage, as similar formulations are widely used in cancer chemotherapies, as evidenced by the use of doxorubicin and daunorubicin via liposomes.[39] It should be noted that while druglikeness guidelines, such as Lipinski's rule of 5,[40] establish a basis for desirable parameter values for active compounds, in this particular case, the guidelines did not fully apply as increased lipophilicity was needed for a better interaction with the target and improve antiproliferative activity.

Conclusion

A general overview of the SAR as antimigratory and antiproliferative agents is shown on **Fig. 9**. As general tendency compounds displaying better antiproliferative activity tend to have long tails, with or without the 1,2,3-triazole moiety. That is markedly different for the best antimigratory activity were the most active analogs are S-alkylated with short aliphatic tails.

The three most active antiproliferative compounds (**9**, **15** and **22**) contained a flexible 16-carbon aliphatic chain, that based on then docking results, enhance the lipophilic interaction with the enzyme. These compounds showed lower estimated free binding energies of than salirasib and the peptide substrate. This suggests that the antiproliferative activity may be linked to an ICMT inhibition mechanism.
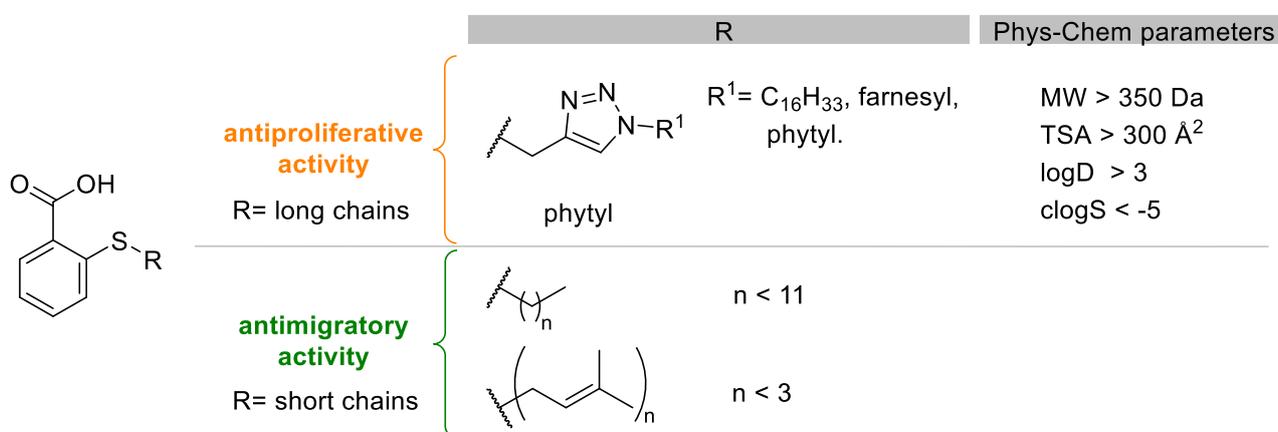
Fig 9. Structure-activity relationship of our library as antiproliferative and antimigratory agents.

Compounds **2**, **3** and **11** display the most intense antimigratory activity. In agreement with our hypothesis, the presence of shorter R chains and the absence of a triazole linker reduced the predicted binding affinity for ICMT. These results suggest that compounds **2**, **3** and **11** may be acting on other molecular targets involved in the regulation of prenylated proteins.

Although the physicochemical parameters may not be ideal for oral dosage, other administration routes, such as intravenous or liposomal delivery, should be explored.

In summary, we were able to demonstrate that modifying the lipophilic moiety of salirasib can enhance its antiproliferative activity. Compounds **9**, **15**, and **22** showed enhanced antiproliferative activity and compounds **2**, **3**, and **11** exhibited specific antimigratory activity. The difference in behaviour is directly linked to the length of the lipophilic tail on the thiosalicylate and the presence of triazoles. Long chains and triazoles are present on antiproliferative active derivatives and short chains are linked to antimigratory activity. (**Fig 9**)

The combination of antiproliferative and antimigratory agents could provide a more integrated treatment approach, where tumor cells are reduced, and metastasis is blocked. The study opens the possibility of developing combination therapies where lipophilic thiosalycilates with antiproliferative and antimigratory activities act together.

Materials and Methods

General method for the preparation of S-alkylated thiosalicylic acid compounds

Thiosalicylic acid (1 equivalent) was dissolved in anhydrous acetone (10 mL/eq), under constant stirring and inert atmosphere. Next, guanidinium carbonate (1 equivalent) and organobromide compound (1 equivalent) were added. The reaction mixture was brought to reflux for 8 hours. To finish the reaction, a solution of 1M HCl was added, continuing to extract the compound of interest with ethyl ether (3 x 25 mL). Combined organic extracts were dried with sodium sulphate and evaporated. Products **1** - **13** were purified by column chromatography in silica gel with increasing hexanes/ethyl acetate gradients (**1**- R=propargyl: 81%; **2**- R=octyl: 83%; **3**- R=decyl: 81%; **4**- R=cyclohexyl: 87%; **5**- R=$CH_2CH_2COCH_2CH_2$: 78%; **6**- R=benzyl: 73%; **7**- R=3-phenylpropyl: 75%; **8**- R=cynnamyl: 68%; **9**- R=phytyl: 85%; **10**- R=prenyl: 72%; **11**- R=geranyl: 88%; **12**- R=farnesyl: 79%; **13**- R=geranylgeranyl: 85%). Full characterization of the products was previously reported.[23]

General procedure for the Cu(I) mediated 1,3-dipolar cycloaddition (CuAAC)

Alkyne **1** (1 equivalent) and azide (1.5 equivalent) were suspended in 10 mL/eq of tBuOH:H$_2$O (1:1). Then, 1 M CuSO4 solution (0.05 equivalents) and 1 M sodium ascorbate solution (0.2 equivalents) were added, and the mixture stirred overnight at room temperature. Brine (30 mL) was added, and the solution was extracted with dichloromethane (3 x 25 mL). Combined organic extracts were dried over sodium sulfate and evaporated. Products **14** – **25** were purified by column chromatography in silica gel with increasing hexane/ethyl acetate gradients (**14-** R=octyl: 78%; **15-** R=cetyl: 81%; **16-** R=cyclohexyl: 84%; **17-** R= CH$_2$COCH$_2$CH$_2$: 92%; **18-** R= CH$_2$CH$_2$COCH$_2$CH$_2$: 91%; **19-** R=benzyl: 80%; **20-** R=3-phenylpropyl: 88%; **21-** R=cynnamyl: 86%; **22-** R=phytyl: 83%; **23-** R=prenyl: 89%; **24-** R=geranyl: 84%; **25-** R=farnesyl: 90%). Full characterization of the products was previously reported.[23]

General procedure for in vitro antiproliferative activity

In vitro antiproliferative activities of the compounds were evaluated using the protocol of the National Cancer Institute of the United States.[41] A panel of six human solid tumor cell lines was used:

A549: adenocarcinomic human alveolar basal epithelial cells, extracted from cancerous lung tissue in the explanted tumor of a 58-year-old Caucasian male (non-small cell lung cancer);

SW1573: alveolar cell carcinoma extracted from a 44-year-old white female (non-small cell lung cancer);

HeLa: cervical cancer cells extracted from Henrietta Lacks, a 31-year-old African American female (cervix cancer);

HBL-100: extracted from the milk of a 27-year-old Caucasian nursing mother and obtained 3 days after delivery (breast cancer);

T-47D: isolated from a pleural effusion obtained from a 54-year-old female patient with an infiltrating ductal carcinoma of the breast (breast cancer).

H1299: extracted from a lymph node metastasis from a non-small cell lung carcinoma 43-year-old white male patient who received prior radiation therapy.

Cells were maintained in RPMI 1640 supplemented with 5% heat-inactivated fetal calf serum, and 2 mM L-glutamine in a 37 ºC, 5% CO$_2$, 95% humidified air incubator. Exponentially growing cells were trypsinized

and re-suspended in antibiotic-containing medium (100 units penicillin G and 0.1 mg of streptomycin per mL). Single-cell suspensions displaying > 97% viability by trypan blue dye exclusion were subsequently counted and plated on 96-well microtiter plates. Cells were inoculated in a volume of 100 µL per well at densities of 2500 (A549, HBL-100, HeLa, SW1573 and H1299) or 5000 (T-47D) cells per well, based on their doubling times. Compounds were dissolved in DMSO at an initial concentration of 40 mM. Control cells were exposed to an equivalent concentration of DMSO (0.25% v/v, negative control). Each compound was tested in triplicate at different dilutions in the range 1–100 µM. Cisplatin, etoposide, camptothecin were used as positive controls. The drug treatment was started on day 1 after plating. Drug incubation times were 48 h, after which time cells were precipitated with 25 µL ice-cold TCA (50% w/v) and fixed for 60 min at 4 ºC. Then the sulforhodamine B (SRB) assay was performed.[42] The optical density (OD) of each well was measured at 530 nm, using BioTek's PowerWave XS Absorbance Microplate Reader. Values were corrected for background OD from wells only containing medium. Antiproliferative activity of the compounds was expressed as GI_{50}, that is, the concentration of the compound that inhibits 50% of the culture growth.

Wound healing assay

H1299 cells maintained in RPMI 1640 supplemented with 10 % heat-inactivated fetal calf serum, antibiotics (100 units penicillin G and 0.1 mg of streptomycin per mL) and 2 mM L-glutamine were plated at high density in 35 mm plates. The following day a scratch was mechanically performed. Culture media was changed to start treatment with each compound at 50 µM concentration, or the corresponding DMSO dilution (0.2 % v/v) as control condition. Wound images were obtained by inverted microscopy for each condition at the initial time, and wound closure was monitored and imaged after 24 h by inverted microscopy. Relative migration was quantified as the area of the wound occupied by cells upon 24 h in each case, comparing with the control condition. Data are expressed as the mean ± s.e.m. and are representative of at least three independent experiments. Unless otherwise indicated, results were analyzed using Student's T–test on two experimental groups. In all cases, p values lower than 0.05 were considered statistically significant.

Invasion assay

Exponentially growing cells were resuspended in RPMI 1640 medium with antibiotics (100 units penicillin G and 0.1 mg of streptomycin per mL) and 2 mM L-glutamine, without FBS, supplemented with the compound of interest at 50 µM concentration, or the corresponding DMSO dilution (0.2 % v/v) as control condition. Cells

were then plated in Matrigel-coated inserts (Corning) at a density of 90,000 cells/well. The lower chamber was filled with complete RPMI medium. Upon 24 h incubation cells on the upper face of the insert were removed mechanically and invading cells on the bottom face were fixed with 4% w/v PFA and stained with methylene blue (Sigma). Cells were quantified from microscope images using ImageJ FIJI software (National Institutes of Health, USA). Data are expressed as the mean ± s.e.m. and are representative of at least three independent experiments. Unless otherwise indicated, results were analyzed using Student's T–test on two experimental groups. In all cases, p values lower than 0.05 were considered statistically significant.

Reported inhibitors and synthetic library database and physicochemical properties prediction

A search of *Hs*ICMT inhibitors was carried out using the ChemBL database.[26,43] Filters on target (ICMT), Organism (*Homo sapiens*), and inhibitory activity (< 100 µM) were applied. This database consists of a total on 467 reported *Hs*ICMT inhibitors. Relevant physicochemical properties (Total Molweight, cLogP, cLogS, and Total Surface Area) were predicted using the Osiris DataWarrior platform.[27] For our synthetic library of salirasib analogues, SMILES of the 25 farnesylthiosalicylic acid (FTS) compounds were used to calculate the *in silico* physicochemical properties. Also, for this collection of FTS analogues, LogD were predicted, using the online ChemAxon LogD predictor.[32]

ADME-Tox predictions

Computational modelling to estimate the bioavailability, aqueous solubility, human intestinal absorption, metabolism, mutagenicity, toxicity, etc. for the compounds were performed using SwissADME,[36] pkCSM [38] and Biotransformer.[37]

SwissADME: The SMILES of compounds **1** - **25** were uploaded to SwissADME (http://www.swissadme.ch/). The following parameters were calculated: *Physicochemical Properties* (Formula, MW, Num. heavy atoms, Num. arom. heavy atoms, Fraction Csp3, Num. rotatable bonds, Num. H-bond acceptors, Num. H-bond donors, Molar Refractivity and TPSA); *Lipophilicity* (Log Po/w (iLOGP), Log Po/w (XLOGP3), Log Po/w (WLOGP), Log Po/w (MLOGP), Log Po/w (SILICOS-IT) and Consensus Log Po/w); *Water Solubility* (Log S (ESOL), Solubility, Class, Log S (Ali), Solubility, Class, Log S (SILICOS-IT), Solubility and Class); *Pharmacokinetics* (GI absorption, BBB permeant, P-gp substrate, CYP1A2 inhibitor, CYP2C19 inhibitor, CYP2C9 inhibitor, CYP2D6 inhibitor, CYP3A4 inhibitor and Log Kp -skin permeation-);

Druglikeness (Lipinski, Ghose, Veber, Egan, Muegge and Bioavailability Score); *Medicinal Chemistry* (PAINS, Brenk, Lead likeness and Synthetic accessibility).

pkCSM: The SMILES of compounds **1** - **25** were uploaded to pkCSM (http://biosig.unimelb.edu.au/pkcsm/prediction), through a *.txt SMILE file. The following parameters were calculated: *Absorption* (Water solubility, Caco2 permeability, Intestinal absorption (human), Skin Permeability, P-glycoprotein substrate, P-glycoprotein I inhibitor, P-glycoprotein II inhibitor); *Distribution* (VDss (human), Fraction unbound (human), BBB permeability, CNS permeability); *Metabolism* (CYP2D6 substrate, CYP3A4 substrate, CYP1A2 inhibitior, CYP2C19 inhibitior, CYP2C9 inhibitior, CYP2D6 inhibitior, CYP3A4 inhibitior); *Excretion* (Total Clearance, Renal OCT2 substrate); *Toxicity* (AMES toxicity, Max. tolerated dose (human), hERG I inhibitor, hERG II inhibitor, Oral Rat Acute Toxicity (LD50), Oral Rat Chronic Toxicity (LOAEL), Hepatotoxicity, Skin Sensitisation, *T.Pyriformis* toxicity, Minnow toxicity).

Biotransformer: The SMILES of compounds **2**, **3**, **9**, **11**, **12**, **13**, **14**, **15**, **22** and **25** were uploaded to Biotransformer (http://biotransformer.ca/). The metabolites prediction was performed for one-step CYP450 catalyzed reactions.

Docking Analysis

The three-dimensional structures of HsICMT (UniProt ID: O60725) was generated using AlphaFold 2,[33] a deep learning-based protein structure prediction algorithm. Computational docking simulations were conducted using the web services SwissDock (http://www.swissdock.ch). This web service is based on the EADock DSS (Evolutionary Algorithm for Docking) software.[44] Evolutionary algorithms are iterative stochastic optimization procedures in which an initial population of solutions is generated and evaluated with respect to a set of constraints described by the fitness function. The algorithm consists of the following steps: many binding modes are generated either in a box (local docking) or in the vicinity of all target cavities (blind docking); simultaneously, their CHARMM energies are estimated on a grid; then, the binding modes with the most favorable energies are evaluated with FACTS, and clustered; and finally, the most favorable clusters can be visualized online and downloaded on your computer.

For the ICMT – inhibitors docking studies, the input target consisted of the *Hs*-ICMT structure modeled from the *Tribolium castaneum* ICMT, PDB code: 5V7P (ICMT-monobody) and 5VG9 (ICMT alone).[45] Compounds **15**, **22** and salirasib (compound **12**) were considered to be inhibitors, and N-MeGly-Ala-Cys-S-

Farnesyl was considered to be a ligand. Their input files for the SwissDock server were generated with Chem3DPro 16.0 and then converted into the ".mol2" format with UCSF Chimera.[46] The docking studies were performed using a clustering RMSD (root mean square deviation, parameter used to discard redundant solutions) of 4.0 Å. All the simulations were conducted without specifying a region of interest (ROI) to ensure that the chosen docking methods could locate the correct binding pocket.

Many criteria from docking results can be used for estimating binding affinity including, free-binding energy (ΔG), full-fitness score, hydrogen binding and total free energy. In our study, we chose the free-binding energy as the main criterion for ranking the most powerful ligands. The lower estimated free energy of binding indicates the higher binding affinity. The docking results with the highest binding score was visualized to assess the molecular interactions with the aid of the UCSF Chimera software package v1.10.

References

[1]   International Agency for Research on Cancer - WHO, "Global Cancer Observatory," can be found under https://gco.iarc.fr/, **n.d.**

[2]   C. M. Borini Etichetti, E. Arel Zalazar, N. Cocordano, J. Girardini, *Front Oncol* **2020**, *10*, 2389.

[3]   N. Berndt, A. D. Hamilton, S. M. Sebti, *Nat Rev Cancer* **2011**, *11*, 775–791.

[4]   W. S. Yang, S. G. Yeo, S. Yang, K. H. Kim, B. C. Yoo, J. Y. Cho, *Amino Acids* **2017**, *49*, 1469–1485.

[5]   H. Y. Lau, M. Wang, *Small GTPases* **2018**, *11*, 271–279.

[6]   I. A. Prior, F. E. Hood, J. L. Hartley, *Cancer Res* **2020**, *80*, 2669–2974.

[7]   I. Cushman, P. J. Casey, *Journal of Biological Chemistry* **2009**, *284*, 27964–27973.

[8]   F. Mantovani, L. Collavin, G. Del Sal, *Cell Death Differ* **2019**, *26*, 199–212.

[9]   C. B. Etichetti, C. Di Benedetto, C. Rossi, M. V. Baglioni, S. Bicciato, G. Del Sal, M. Menacho-Marquez, J. Girardini, *Journal of Biological Chemistry* **2019**, *294*, 5060–5073.

[10]   S. M. Sebti, A. D. Hamilton, *Oncogene* **2000**, *19*, 6584–6593.

[11]   "Study of Tipifarnib in Patients With Previously-Treated, Advanced, HRAS Mutant Urothelial Carcinoma," can be found under https://clinicaltrials.gov/ct2/show/NCT02535650, **n.d.**

[12]   I. Mohammed, S. E. Hampton, L. Ashall, E. R. Hildebrandt, R. A. Kutlik, S. P. Manandhar, B. J. Floyd, H. E. Smith, J. K. Dozier, M. D. Distefano, W. K. Schmidt, T. M. Dore, *Bioorg Med Chem* **2016**, *24*, 160–178.

[13]   A. M. Wahlstrom, B. A. Cutts, C. Karlsson, K. M. E. Andersson, M. Liu, A. K. M. Sjogren, B. Swolin, S. G. Young, M. O. Bergo, *Blood* **2007**, *109*, 763–768.

[14]   A. M. Winter-Vann, R. A. Baron, W. Wong, J. Dela Cruz, J. D. York, D. M. Gooden, M. O. Bergo, S. G. Young, E. J. Toone, P. J. Casey, *Proc Natl Acad Sci U S A* **2005**, *102*, 4336–4341.

[15]   D. Marciano, G. Ben-Baruch, M. Marom, Y. Egozi, R. Haklai, Y. Kloog, *J Med Chem* **1995**, *38*, 1267–1272.

[16]   M. Marom, R. Haklai, G. Ben-Baruch, D. Marciano, Y. Egozi, Y. Kloog, *J Biol Chem* **1995**, *270*, 22263–22270.

[17]   G. Elad, A. Paz, R. Haklai, D. Marciano, A. Cox, Y. Kloog, *Biochim Biophys Acta* **1999**, *1452*, 228–242.

[18]   M. Gana-Weisz, J. Halaschek-Wiener, B. Jansen, G. Elad, R. Haklai, Y. Kloog, *Clinical Cancer Research* **2002**, *8*, 555–565.

[19]   J. Furuse, T. Kurata, N. Okano, Y. Fujisaka, D. Naruge, T. Shimizu, H. Kitamura, T. Iwasa, F. Nagashima, K. Nakagawa, *Cancer Chemother Pharmacol* **2018**, *82*, 511–519.

[20] G. J. Riely, M. L. Johnson, C. Medina, N. A. Rizvi, V. A. Miller, M. G. Kris, M. C. Pietanza, C. G. Azzoli, L. M. Krug, W. Pao, M. S. Ginsberg, *Journal of Thoracic Oncology* **2011**, *6*, 1435–1437.

[21] J. A. Bergman, K. Hahne, J. Song, C. A. Hrycyna, R. A. Gibbs, *ACS Med Chem Lett* **2012**, *3*, 15–19.

[22] Y. Xiong, T. Hou, L. Liu, W. Peng, C. Wang, Y. Lu, S. Wang, J. Shi, S. Song, *Int J Pharm* **2019**, *572*, 118823.

[23] E. O. J. Porta, I. Bofill Verdaguer, C. Perez, C. Banchio, M. Ferreira De Azevedo, A. M. Katzin, G. R. Labadie, *Medchemcomm* **2019**, *10*, 1599–1605.

[24] E. O. J. Porta, M. M. Vallejos, A. B. J. Bracca, G. R. Labadie, *RSC Adv* **2017**, *7*, 47527–47538.

[25] E. O. J. Porta, S. N. Jäger, I. Nocito, G. I. Lepesheva, E. C. Serra, B. L. Tekwani, G. R. Labadie, *Medchemcomm* **2017**, *8*, 1015–1021.

[26] D. Mendez, A. Gaulton, A. P. Bento, J. Chambers, M. De Veij, E. Félix, M. P. Magariños, J. F. Mosquera, P. Mutowo, M. Nowotka, M. Gordillo-Marañón, F. Hunter, L. Junco, G. Mugumbate, M. Rodriguez-Lopez, F. Atkinson, N. Bosc, C. J. Radoux, A. Segura-Cabrera, A. Hersey, A. R. Leach, *Nucleic Acids Res* **2019**, *47*, D930–D940.

[27] T. Sander, J. Freyss, M. Von Korff, C. Rufener, *J Chem Inf Model* **2015**, *55*, 460–473.

[28] INC. SIGNUM BIOSCIENCES, M. VORONKOV, J. STOCK, M. STOCK, S.-Y. LEE, E. PEREZ, J. GORDON, *Anti-Inflamatory Complexes*, **2010**, WO 2010/090845 A1.

[29] INC. SIGNUM BIOSCIENCES, M. VORONKOV, E. PEREZ, J. HEALY, J. FERNANDEZ, *Compounds and Methods Use*, **2018**, WO 2018/132759 A1.

[30] S. Sugita, H. Enokida, H. Yoshino, K. Miyamoto, M. Yonemori, T. Sakaguchi, Y. Osako, M. Nakagawa, *Int J Oncol* **2018**, *53*, 725–736.

[31] L. Lang, C. Shay, X. Zhao, Y. Teng, *Journal of Experimental and Clinical Cancer Research* **2017**, *36*, DOI 10.1186/s13046-017-0583-4.

[32] "ChemAxon Calculator and Predictors," can be found under https://chemaxon.com/products/calculators-and-predictors, **n.d.**

[33]   J. Jumper, R. Evans, A. Pritzel, T. Green, M. Figurnov, O. Ronneberger, K. Tunyasuvunakool, R. Bates, A. Žídek, A. Potapenko, A. Bridgland, C. Meyer, S. A. A. Kohl, A. J. Ballard, A. Cowie, B. Romera-Paredes, S. Nikolov, R. Jain, J. Adler, T. Back, S. Petersen, D. Reiman, E. Clancy, M. Zielinski, M. Steinegger, M. Pacholska, T. Berghammer, S. Bodenstein, D. Silver, O. Vinyals, A. W. Senior, K. Kavukcuoglu, P. Kohli, D. Hassabis, *Nature* **2021**, *596*, 583–589.

[34]   L. P. Wright, H. Court, A. Mor, I. M. Ahearn, P. J. Casey, M. R. Philips, *Mol Cell Biol* **2009**, *29*, 1826–1833.

[35]   M. M. Diver, L. Pedi, A. Koide, S. Koide, S. B. Long, *Nature* **2018**, *553*, 526–529.

[36]   A. Daina, O. Michielin, V. Zoete, *Sci Rep* **2017**, *7*, 42717.

[37]   Y. Djoumbou-Feunang, J. Fiamoncini, A. Gil-de-la-Fuente, R. Greiner, C. Manach, D. S. Wishart, *J Cheminform* **2019**, *11*, 2.

[38]   D. E. V. Pires, T. L. Blundell, D. B. Ascher, *J Med Chem* **2015**, *58*, 4066–4072.

[39]   S. M. Rafiyath, M. Rasul, B. Lee, G. Wei, G. Lamba, D. Liu, **2012**.

[40]   C. A. Lipinski, F. Lombardo, B. W. Dominy, P. J. Feeney, *Adv Drug Deliv Rev* **2001**, *46*, 3–26.

[41]   P. Skehan, R. Storeng, D. Scudiero, A. Monks, J. Mcmahon, D. Vistica, J. T. Warren, H. Bokesch, S. Kenney, M. R. Boyd, *J Natl Cancer Inst* **1990**, *82*, 1107–1112.

[42]   P. O. Miranda, J. M. Padrón, J. I. Padrón, J. Villar, V. S. Martín, *ChemMedChem* **2006**, *1*, 323–329.

[43]   M. Davies, M. Nowotka, G. Papadatos, N. Dedman, A. Gaulton, F. Atkinson, L. Bellis, J. P. Overington, *Nucleic Acids Res* **2015**, *43*, W612–W620.

[44]   A. Grosdidier, V. Zoete, O. Michielin, *Nucleic Acids Res* **2011**, *39*, W270–W277.

[45]   M. Mirdita, L. Von Den Driesch, C. Galiez, M. J. Martin, J. Soding, M. Steinegger, *Nucleic Acids Res* **2017**, *45*, D170–D176.

[46]   E. F. Pettersen, T. D. Goddard, C. C. Huang, E. C. Meng, G. S. Couch, T. I. Croll, J. H. Morris, T. E. Ferrin, *Protein Science* **2021**, *30*, 70–82.